Theor. Appl. Climatol. 82, 225–243 (2005)
DOI 10.1007/s00704-005-0132-5

Theoretical and Applied Climatology
Printed in Austria

[1] School of Earth and Atmospheric Sciences, Georgia Institute of Technology, Atlanta, GA, USA
[2] Department of Environmental Science, Policy and Management, University of California, Berkeley, CA, USA
[3] Physics of Weather and Climate Group, International Centre for Theoretical Physics, Trieste, Italy

The coupling of the Common Land Model (CLM0) to a regional climate model (RegCM)

A. L. Steiner[1,2], **J. S. Pal**[3], **F. Giorgi**[3], **R. E. Dickinson**[1], and **W. L. Chameides**[1]

With 8 Figures

Received May 11, 2004; revised January 13, 2005; accepted January 16, 2005
Published online May 20, 2005

Summary

We replace the existing land surface parameterization scheme, the Biosphere-Atmosphere Transfer Scheme (BATS), in a regional climate model (RegCM) with the newly developed Common Land Model (CLM0). The main improvements of CLM0 include a detailed 10-layer soil model, the distinction between soil ice and water phases, a linked photosynthesis-stomatal conductance model, a multilayer snow model, and an improved runoff parameterization. We compare the performance of CLM0 and BATS as coupled to the RegCM in a one year simulation over East Asia. We find that the RegCM/CLM0 improves the winter cold bias present in the RegCM/BATS simulation. With respect to the surface energy balance, lower CLM0 albedos allow the absorption of more solar radiation at the surface. CLM0 tends to simulate higher sensible heat and lower latent heat fluxes than its BATS counterpart. The surface water balance also changes considerably between the two land surface schemes. Compared to BATS, CLM0 precipitation is reduced overall and surface runoff is increased, thereby allowing less water to enter the soil column. Evapotranspiration is lower in CLM0 due to lower ground evaporation, which leads to a wetter surface soil in CLM0 in spite of less precipitation input. However, transpiration is greater in CLM0 than BATS, which has an overall effect of less surface storage during the summertime. Comparison with station observations indicates that CLM0 tends to improve the simulation of root zone soil water content compared to BATS. Another pronounced difference between the two schemes is that CLM0 produces lower snow amounts than BATS because of different snow models and warmer CLM0 temperatures. In this case, BATS snow cover amounts are more in line with observations. Overall, except for the snow amounts, CLM0 appears to improve the RegCM simulation of the surface energy and water budgets compared to BATS.

1. Introduction

The land-atmosphere interface in global climate models supplies the model's lower boundary condition for more than 30% of the Earth's surface (Henderson-Sellers and Dickinson, 1993), and this percentage can be even greater for regional climate modeling domains. The description of this boundary condition can significantly impact the transfer of mass, momentum and energy between the atmosphere and the land surface. This can, in turn, affect prognostic variables such as surface temperature, precipitation, and the vertical distribution of atmospheric water vapor and clouds. In this study over East Asia, we evaluate the impact of replacing the current land surface parameterization (BATS, Dickinson et al., 1993) in a regional climate model (RegCM, Giorgi et al., 1993a, b) with the newly developed Common Land Model (CLM) (Dai et al., 2003).

Land surface parameterizations, which use a set of mass and energy balance equations to characterize the surface fluxes, have undergone a series of developments over the past several decades (Sellers et al., 1997). The first generation models used aerodynamic bulk transfer formulas to describe the energy balance along with a simple ''bucket'' model (Manabe, 1969) to account for soil moisture variability. Second generation models introduced vegetation and its impact on radiation, momentum transfer, and evapotranspiration. The current land surface model in the RegCM, the Biosphere-Atmosphere Transfer Scheme (BATS) (Dickinson et al., 1993), is an example of a second-generation model. The most current models, the third generation, add a linked photosynthesis-stomatal conductance model to realistically simulate the observed relationship between photosynthesis and transpiration. An example of a recently developed third generation model is the Common Land Model (CLM) (Dai et al., 2003). The CLM is a community model developed to compile and improve upon several components of the most widely used land surface schemes for use with the National Center for Atmospheric Research (NCAR) Community Climate System Model (CCSM). Previous CLM studies include an offline validation study (Dai et al., 2003) and the coupling with a global climate model (CCM3) (Zeng et al., 2002; Bonan et al., 2002).

Here, we upgrade the land surface model in the RegCM from a second generation model (BATS) to a third generation model (CLM) and investigate the impact of the new land surface scheme upon regional climate model simulations. We focus on East Asia in order to utilize the coupled model in a future study, which will evaluate the impacts of high concentrations of anthropogenically-produced aerosols on vegetation and other surface parameters in the region. The BATS scheme is replaced with its CLM successor in order to benefit from the improved surface hydrology, surface energy balances, and the inclusion of a stomatal conductance-photosynthesis model. This paper provides a preliminary evaluation of the performance of the CLM versus the previous land surface parameterization (BATS) in the RegCM as a prelude to future climate change and sensitivity studies.

2. Model description

2.1 The regional climate model (RegCM)

The regional climate model RegCM used in the present study is described in detail by Giorgi et al. (1993a, b), Giorgi and Shields (1999), Giorgi et al. (1999) and Pal et al. (2000). It is a grid-point limited area model with a dynamical core essentially the same as that of the hydrostatic version of the NCAR/PSU MM5 (Grell et al., 1993). The boundary layer scheme is from Holtslag et al. (1990) while the radiative transfer calculations are carried out using the CCM3 radiation package (Kiehl et al., 1996). Radiation is calculated using a delta-Eddington approximation (Briegleb, 1992) and takes into account greenhouse gases (H_2O, CO_2, O_3, CH_4, N_2O and CFCs), cloud ice effects and radiative effects of a specified distribution of background atmospheric aerosols. Precipitation is parameterized for resolvable-scale precipitation using the Pal et al. (2000) scheme and for convective precipitation using the Kuo-type scheme of Anthes (1977) and Anthes et al. (1987). In our study, BATS is replaced by the CLM scheme described below. Differences in the two land surface schemes are detailed in section 2.3.

2.2 CLM0 model description

The CLM is a land surface model based on the physical components of three existing land surface models: the BATS scheme (the land surface package currently implemented in the RegCM), the Land Surface Model (LSM) (Bonan et al., 1996), and the snow model of Dai and Zeng (1996) (IAP94). The CLM was developed to utilize the best aspects of each of these three codes and combined them to form a state-of-the-art land surface parameterization for use in climate models. The CLM calculates the land surface variables at each model grid point with ten unevenly spaced soil layers, one vegetation layer with a canopy photosynthesis-conductance model, and up to five snow layers depending upon the total snow depth. Soil temperature and soil moisture are solved with explicit treatment of liquid water and ice. Runoff is calculated from surface and base flow for saturated and unsaturated regions and is roughly based on the principles of TOPMODEL (Stieglitz et al., 1997). Ocean surface fluxes are calculated from

bulk transfer coefficients. The CLM has the additional ability to include subgrid "tiles," with a separate water and energy balance conducted for each tile, following the "mosaic" approach of Koster and Suarez (1992). These tile values are then area-weighted before returning grid values to the atmospheric model. Further model details are presented in Dai et al. (2003) and differences between the CLM and BATS parameterizations are detailed below. Additionally, the code was designed to accommodate satellite-derived land surface data and can be used with various land surface classification schemes. Here we implement CLM version 0 (hereinafter referred to as CLM0), as described by Dai et al. (2003) and Zeng et al. (2002).

2.3 Differences between CLM0 and BATS parameterizations

BATS and CLM0 have several common components but also some significant differences. The key differences are summarized below.

1. Surface representation: CLM0 has a total of ten vertical soil levels, up to five snow levels, and one vegetation level. Soil characteristics in CLM0, such as soil thermal and hydraulic properties, are based on the percentage of sand, silt and clay in the soil (Clapp and Hornberger, 1978). BATS has three soil moisture levels, two soil temperature levels, one snow layer that is combined with the surface soil layer in the temperature calculations, and one vegetation layer. BATS uses pre-defined soil texture categories to determine soil properties, although these soil texture categories are roughly based on the same soil descriptions from Clapp and Hornberger (1978). In this study, we match CLM0 soil textures, land surface classification, and leaf area index (LAI) values to the BATS categories to provide the same model input for the two schemes.
2. Albedos: CLM0 and BATS use the same albedo parameterization for snow and soil, but different approaches for vegetation albedos. For vegetation, CLM0 uses a modified two-stream approach that reduces the complexity of a full two-stream albedo treatment (Dai et al., 2003). This approach allows the vegetation albedos to equal the underlying ground albedo when LAI is zero and change to the land cover-specific vegetation albedo when LAI reaches a seasonal maximum. BATS uses prescribed values for vegetation albedo for both short- and longwave components based on the BATS land cover types. The prescribed vegetation albedos of CLM0 are based on AVHRR-derived albedo data and tend to be less than the prescribed BATS values (Zeng et al., 2002), and these changes were retained in order to evaluate CLM0 improvements.
3. Surface fluxes: The surface fluxes of momentum, sensible heat, and latent heat are caused by turbulent transport and are simulated using surface layer similarity theory (Brutsaert, 1982). CLM0 and BATS use different surface layer similarity approaches to solve for canopy and bare ground fluxes. In both cases, the turbulent fluxes are first derived for neutral conditions and then modified as needed to account for turbulent conditions using the Monin-Obukhov similarity theory. CLM0 revises the surface stability functions used in the BATS parameterization with an improved treatment of turbulence under free convective conditions (Zeng et al., 1998). Additionally, the aerodynamic resistance to these fluxes varies between model versions via the surface roughness. BATS holds the heat and water vapor roughness lengths constant, while CLM0 updates these values over bare soil and snow with values from the stability functions (Zilitinkevich, 1970; Zeng and Dickinson, 1998). CLM0 also modifies the parameterization of bare soil evaporation to account for a decrease in soil specific humidity as the soil dries, based on the parameterization of Philip (1957).
4. Soil Temperatures and Soil Moisture: Canopy (or leaf) temperatures are calculated in a similar manner in BATS and CLM0. However, the calculation of soil and snow temperatures is quite different between the two models. BATS uses a two-layer force-restore model to calculate soil temperatures (Deardorff, 1978; Dickinson, 1988). When snow is present, a composite soil/snow layer temperature is derived as the surface temperature layer (Yang and Dickinson, 1997). In contrast, the CLM explicitly solves a ten-layer soil model and snow model with up to five layers assuming

a zero heat flux at the lower boundary of the soil column. Heat transfer between each layer is calculated to derive the temperature of each soil and snow layer. Additionally, soil thermal and hydraulic properties are calculated as a function of soil type. Phase changes for soil or snow moisture within each soil and snow layer are allowed.

5. Runoff: Both BATS and CLM0 divide runoff into a surface and base flow term. However, CLM0 includes terms from TOPMODEL (Stieglitz et al., 1997) that relate these terms to the fraction of surface that is saturated as inferred from a modeled water table.
6. Canopy Water Storage: Both schemes model vegetation interception and runoff similarly, but the CLM0 also adds the throughfall of precipitation. Throughfall is dependent upon the leaf and stem area indexes (LSAI) and can add additional moisture to the ground surface.
7. Vegetation Canopy: BATS treats all vegetation within the canopy in the same manner, while CLM0 divides the canopy into sunlit and shaded fractions as a function of LAI using a Lambert-Beer-like formulation for the extinction of light through the canopy (Sellers, 1985; Bonan, 1996). CLM0 also divides the flux of photosynthetically active radiation (PAR) into direct and diffuse portions which is distributed between the sunlit and shaded leaf fractions; i.e. sunlit leaves receive both direct and diffuse light while shaded leaves receive only diffuse radiation. The leaf boundary layer theory is the same between the two schemes.
8. Stomatal Conductance and Photosynthesis: BATS and CLM0 use different stomatal conductance parameterizations. BATS utilizes the method of Jarvis (1976), which calculates stomatal resistance from the minimum stomatal resistance value and light, seasonal, moisture, and vapor pressure deficit factors. BATS does not compute photosynthetic rates. In the CLM0 module, stomatal conductance is calculated for sunlit and shaded fractions and is a function of photosynthetic rate, the CO_2 leaf-surface concentration, and the gradient of water vapor pressure over the leaf surface (Collatz et al., 1991). The photosynthetic rate is calculated as in Farquhar et al. (1980) and Collatz et al. (1991). Both photosynthetic rates and stomatal conductances are calculated separately for sunlit and shaded leaves.
9. Snow: The BATS snow module only considers snow surface properties and groups soil and snow together for the temperature and soil moisture calculations (Yang and Dickinson, 1997). The CLM0 snow module, based on the IAP94 model (Dai and Zeng, 1996), uses up to five snow layers and calculates temperature and moisture explicitly for each layer. These layers have the ability to compact by melting, overburden, or metamorphosis; if these processes occur, the layers can be redivided or combined.

Further model details can be obtained from Dickinson et al. (1993) for BATS and from Dai et al. (2003) for CLM0.

3. Simulation specifics

3.1 Model input parameters

The full simulation period ranges from June 1, 1994 to August 31, 1995 with the same model domain, horizontal resolution, and vertical resolution as in Giorgi et al. (1999). The model grid is composed of 60 km×60 km cells distributed in a horizontal grid of 80 rows and 103 columns which covers much of East Asia (see Fig. 1) in the area approximately enclosed by the coordinates 48.42° N, 84.42° E; 48.66° N, 154.4° E; 14.09° N, 99.43° E; and 14.21° N, 140.1° E. Also shown in Fig. 1 are four subregions selected for more detailed analysis.

To allow for a two-month spinup time period, we analyze the results from August 1, 1994 to August 31, 1995. The model was first run for this period using the BATS land surface model and then repeated for the same time period using the CLM land surface model. The basic climatology over East Asia for this simulation period is discussed for the RegCM/BATS model version in Giorgi et al. (1999). Initial and boundary conditions to drive the atmospheric dynamics are taken from the European Center for Medium-Range Weather Forecast (ECMWF) analysis. Boundary conditions are updated every 6 hours on a T42 grid (Trenberth and Olson, 1992), corresponding to a grid point spacing of approximately 2.89 degrees, for temperature, surface

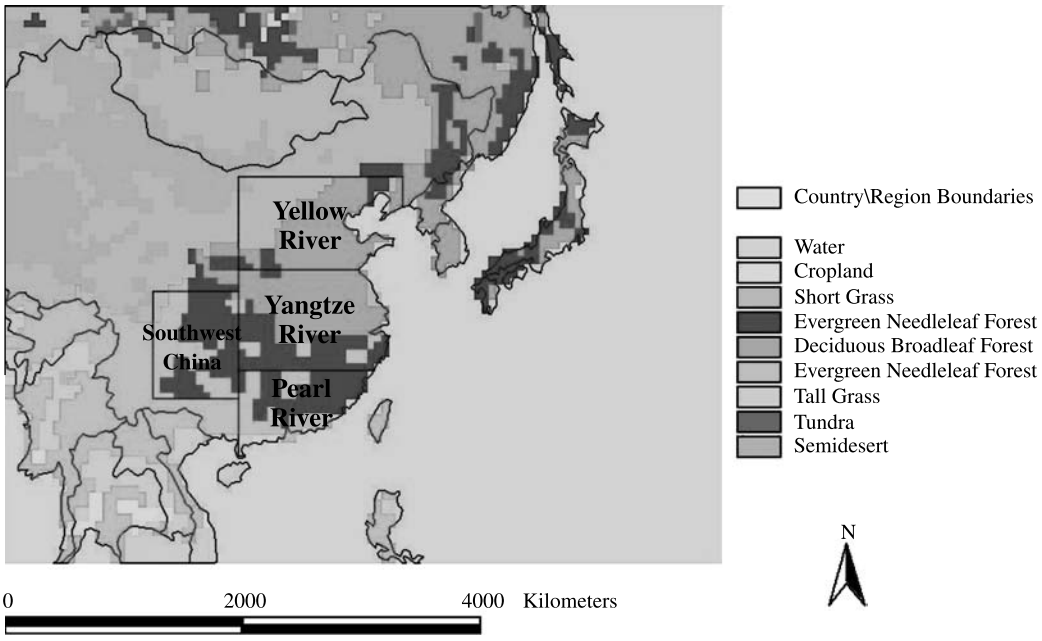

Fig. 1. The China-MAP model domain with BATS land cover categories. Regions here correspond to that of Giorgi et al. (1999). Yellow River = North China, Yangtze River = Central China, Pearl River = South China, and Southwest China. Regions are defined for the analytical purposes of this study

pressure, water vapor and wind at all 14 vertical σ-levels.

For the purpose of this model comparison, several land surface parameters in CLM0 were scaled to those in BATS to provide a better comparison of surface physics. These include a matching of BATS land cover categories to the IGBP categories used by CLM0, as well as the matching of soil color and texture based on the land cover categories. The CLM0 ability to include remotely sensed LAI and fractional vegetation is not utilized in this study in order to allow better consistency with input parameters with BATS. For both schemes, soil moisture is initialized by prescribing the soil water content relative to saturation as a function of land cover type (Giorgi and Bates, 1989).

3.2 Coupling interfaces

Several radiative and atmospheric fields are transferred between the RegCM climate code and the BATS or CLM0 land surface code. CLM0 requires four components of incoming shortwave radiation (visible direct, visible diffuse, near-IR direct, and near-IR diffuse), incoming longwave radiation, precipitation, and the lowest atmospheric model layer height, temperature, wind, pressure, specific humidity and air density. After the land surface model completes the water and energy balance calculations, it returns albedos (visible direct and diffuse, and near-IR direct and diffuse), zenith angle, surface drag coefficient, surface temperature, sensible heat flux, evaporation rate, radiative temperature, and snow. BATS requires the same coupling parameters as CLM0 with the exception of a bulk incoming radiation field instead of individual direct and diffuse components. In the remainder of this paper, we will refer to the experiments including the CLM0 scheme as ‘‘CLM0 simulations,’’ with similar terminology for BATS.

4. Simulation results

4.1 Precipitation

Figure 2 and Table 1 compare precipitation in the BATS and CLM0 simulations with observed precipitation from the Climatic Research Unit (CRU; New et al., 1999, 2000) over the interior domain and the four subregions of Fig. 1. The interior domain is defined here by all land points in the domain after the outermost 20 grid point rows and columns are removed. The CRU dataset is based on station data and provides monthly

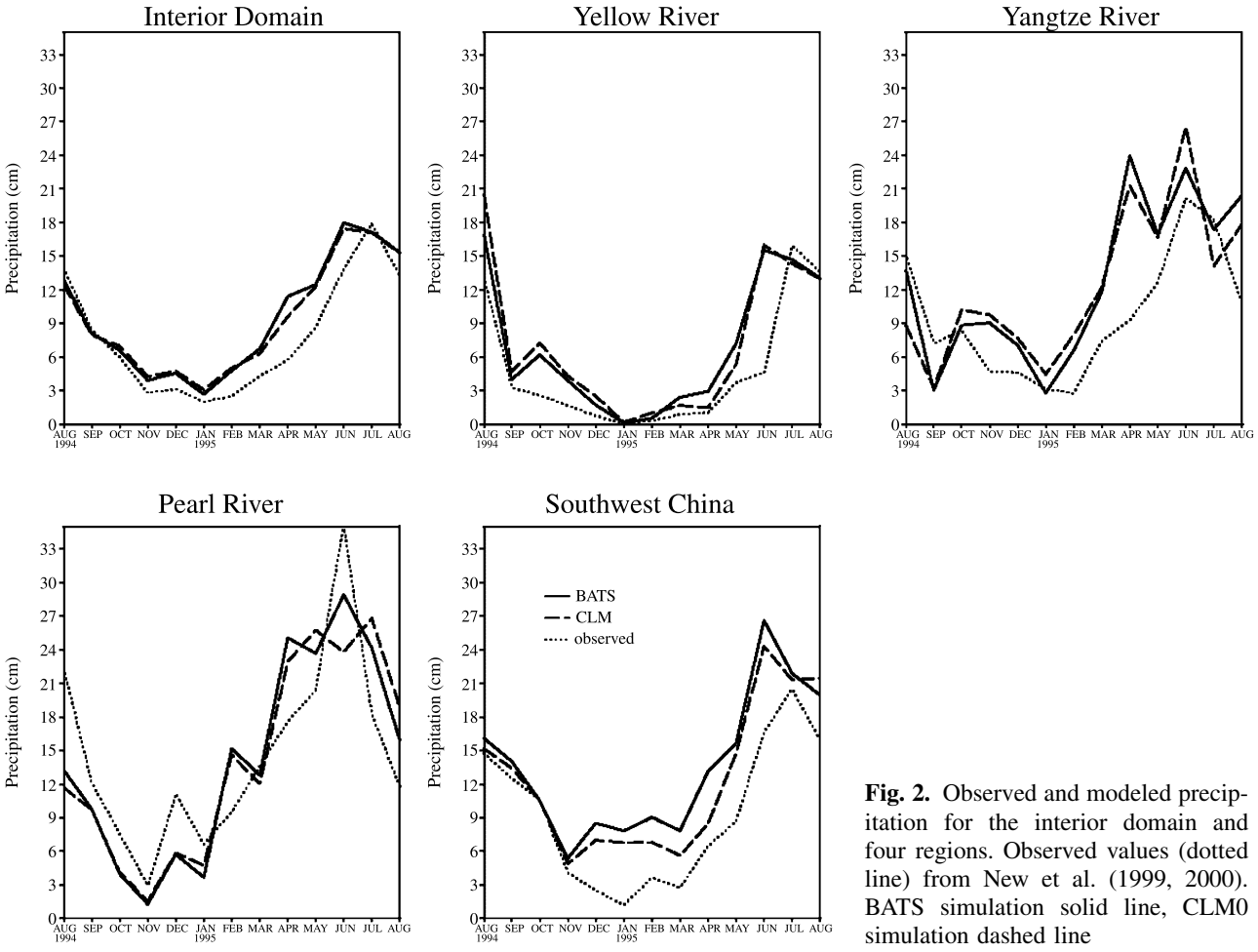

Fig. 2. Observed and modeled precipitation for the interior domain and four regions. Observed values (dotted line) from New et al. (1999, 2000). BATS simulation solid line, CLM0 simulation dashed line

Table 1. Observed (OBS) and Modeled Precipitation (cm/month). Observational data from New et al. (1999, 2000). Positive values indicate a model bias, where modeled precipitation exceeds that of observed precipitation

	Annual			DJF 1994/1995			JJA 1995		
	OBS	BATS-OBS	CLM-OBS	OBS	BATS-OBS	CLM-OBS	OBS	BATS-OBS	CLM-OBS
Interior Domain	7.88	1.70	1.55	2.55	1.45	1.72	15.01	1.80	1.61
Yellow River	4.73	2.14	2.08	0.36	0.43	0.86	11.40	3.04	2.10
Yangtze River	9.60	3.04	3.10	3.51	1.96	3.20	16.44	3.76	3.95
Pearl River	14.87	−1.13	−1.13	8.91	−1.25	−1.01	23.22	−0.23	−0.07
Southwest China	9.26	4.32	3.01	2.45	6.01	4.41	17.71	5.10	4.82

precipitation over land on a 0.5 degree resolution grid with a multi-decadal global uncertainty estimate of 10–25% (New et al., 1999, 2000; Giorgi, 2002). With respect to the treatment of precipitation in the RegCM, the main difference between the simulations reported here and that of Giorgi et al. (1999) is the inclusion of the subgrid cloud and precipitation parameterization of Pal et al. (2000); therefore, some differences may occur between our results and those of Giorgi et al. (1999).

East Asia typically experiences cold, dry winters and warm, wet summers due to the onset and evolution of the East Asia monsoon. The monsoon usually begins in April and May over southeastern China and moves northward to the

Yellow River region and northern China in mid-July, eventually retreating in late August and September (Lau and Li, 1984). Both BATS and CLM0 adequately simulate this seasonal pattern of precipitation, with values ranging from a few centimeters per month in winter to about 20 or more centimeters in the summer. In both simulations, the winter through spring season is generally modeled as too wet, with the exception of the Pearl River region. In the summer, both models tend to have earlier and broader summer precipitation peaks. Some of the high model bias in precipitation could be a consequence of the lack of gauge correction in the CRU data set. A gauge correction accounts for the undercatchment of precipitation in conditions of blowing snow and rain (e.g. Legates and Willmott, 1990; Adams and Lettenmaier, 2003) and can vary from ∼10% in warm climate conditions to ∼20% in cold climate conditions (Giorgi et al., 1999).

In the northern Yellow River region, very little precipitation is observed during the winter (December, January, and February spanning 1994 and 1995). Both the BATS and CLM0 simulations tend to over predict this amount by approximately 1 cm, with the CLM0 simulation improving during the first several months of 1995. In the Yangtze River region during DJF, the CLM0 experiment simulates 50 percent higher precipitation than observed, as opposed to a 35 percent over prediction by the BATS simulation. In Southwest China, the precipitation in the winter months is significantly overestimated in both simulations, though the CLM0 produces about 1.5 cm less precipitation during the winter. Giorgi et al. (1999) commented that the model overestimated precipitation over the entire simulation for this subregion and that a true evaluation of this overestimate is difficult due to the complex topography of the region and paucity of observation data there.

Both simulations capture the summer monsoon precipitation maximum over East Asia, although the timing and magnitude is different than observations. For instance, the model underestimates the magnitude of the summer precipitation peak in the Pearl River region, yet overestimates the magnitude in the Yangtze River and Southwest China regions. In most regions, the modeled onset of the monsoon often occurs one month prior to the observed. Although the summer average precipitation (JJA 1995) is within 1.5–2 cm (∼17%) of that observed for the domain as a whole, the slightly negative bias over the Pearl River and the large positive biases elsewhere may indicate an excessive northward displacement of the monsoon front by the models.

In general, CLM0 produces slightly less precipitation than BATS over the annual cycle and in the summer, and slightly more precipitation in the winter. Inspection of Fig. 2 indicates that the greatest differences between the two simulations occur during June in the Yangtze and Pearl River regions. In the Yangtze River region, CLM0 predicts ∼3 cm more precipitation than BATS, while in the Pearl River region, CLM0 predicts ∼5 cm less than BATS. It is difficult to assess what is causing the variations between these two schemes during this time period. Precipitation changes can be due to differences in convective processes (due to variations in the vertical profile of temperature, water vapor mixing ratio, and stability) or large-scale circulations. We find that both convective and nonconvective precipitation contribute to the excess of CLM0 precipitation predicted in the Yangtze River, while the Pearl River decrease in CLM0 precipitation is predominantly due to convective precipitation. Therefore, it appears that a combination of processes can contribute to these differences between the schemes.

To summarize the precipitation results, the use of CLM0 does not strongly affect the simulation of precipitation in the RegCM in a systematic way, with different regions and seasons receiving either greater or smaller amounts of precipitation. Giorgi and Bi (2000) have shown that the simulated precipitation exhibits a significant level of variability due solely to the nonlinearities in the internal dynamics and physics of the model, so that it is difficult to attribute the changes observed to specific features of the land surface schemes.

4.2 Surface air temperature

In Fig. 3 and Table 2, the simulated surface temperatures are compared with observed surface temperatures from the CRU dataset. Corrections for the CRU temperature were applied to scale for elevation differences, as described by Giorgi et al. (1999), and have a multi-decadal global

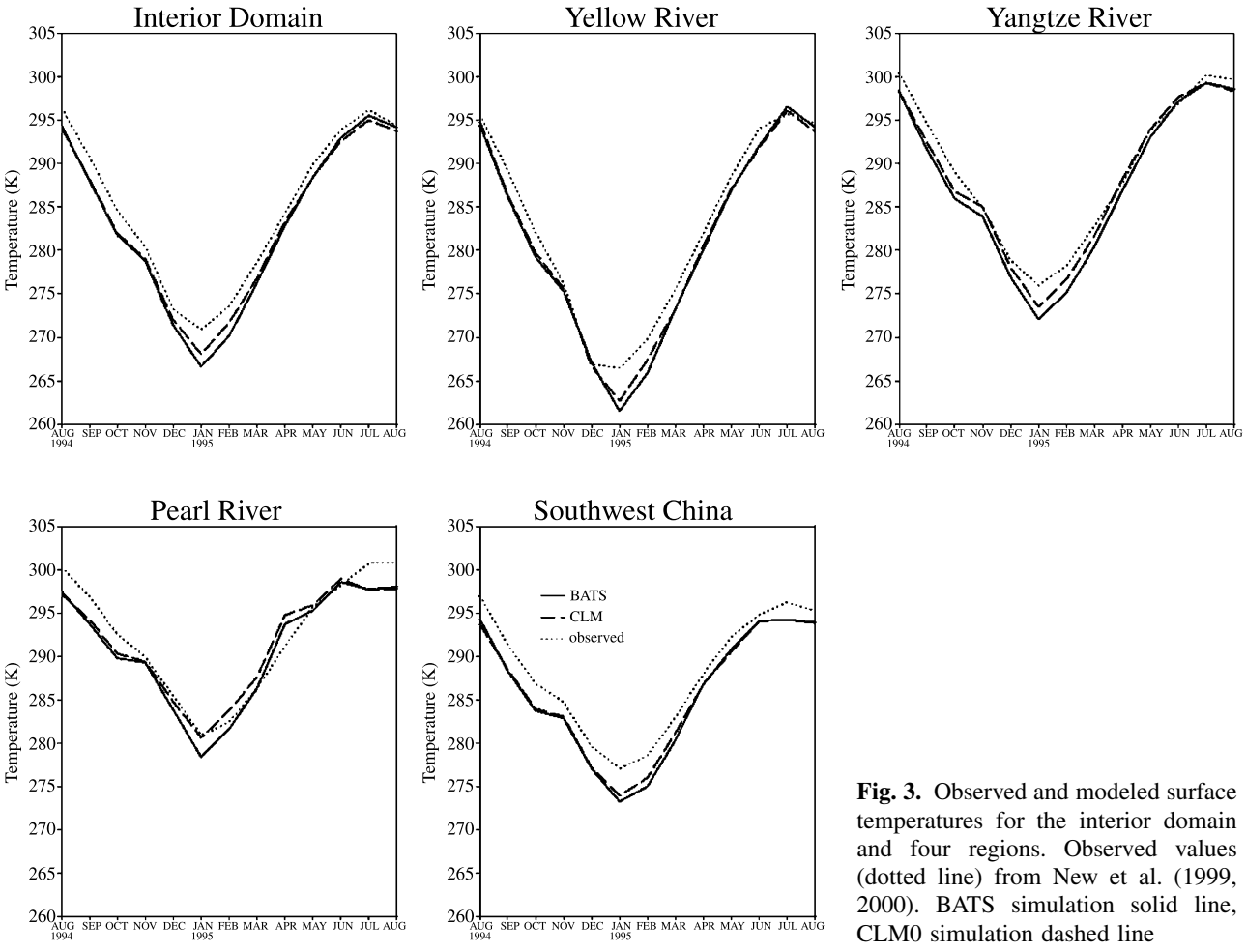

Fig. 3. Observed and modeled surface temperatures for the interior domain and four regions. Observed values (dotted line) from New et al. (1999, 2000). BATS simulation solid line, CLM0 simulation dashed line

Table 2. Observed (OBS) and Modeled Surface Air Temperatures in Kelvin. Observational data from New et al. (1999, 2000). Positive values indicate a model bias, where modeled temperatures exceed that of observed temperatures

	Annual			DJF 1994/1995			JJA 1995		
	OBS	BATS-OBS	CLM-OBS	OBS	BATS-OBS	CLM-OBS	OBS	BATS-OBS	CLM-OBS
Interior Domain	285.16	−1.97	−1.71	269.53	−3.16	−1.98	294.82	−0.58	−1.04
Yellow River	282.82	−1.82	−1.59	267.73	−2.87	−2.13	294.79	−0.51	−0.94
Yangtze River	289.48	−1.82	−0.96	277.69	−2.98	−1.63	298.91	−0.55	−0.26
Pearl River	292.74	−1.31	−0.63	282.94	−0.98	0.71	299.93	−1.67	−1.68
Southwest China	288.05	−2.31	−2.07	278.42	−3.31	−2.72	295.44	−1.37	−1.39

uncertainty of 0.5–1.3 K (New et al., 1999, 2000; Giorgi et al., 2002). Temperatures are underestimated over the interior domain both annually and seasonally in both the BATS and CLM0 simulations, mostly as a result of a winter cold bias of a few degrees. However, the CLM0 winter temperatures are systematically higher than the BATS temperatures and reduce the model winter cold bias by approximately 1 K over the interior domain. Regionally, the winter bias is reduced by 0.5 to 1.5 K in the northern and central regions. This winter cold bias in the BATS simulation was also noted by Giorgi et al. (1999). In the Giorgi et al. (1999) study, the bias was mostly attributed to the simulation of excessive high level cloudiness and possibly the lack of urban heating

effects in the model, and both of these effects could be contributing to the present model bias.

We also examined the differences in daily minimum and daily maximum temperature for both land surface schemes (not shown). Over the annual simulation, the CLM0 simulates a maximum temperature that is 0.5 to 1.5 K greater than BATS, and this difference increases to approximately 2 to 2.5 K in the winter. The average CLM0 minimum temperatures are typically about 0.5 to 1 K less than the BATS simulation, indicating an amplification of the diurnal temperature cycle by CLM0. The Pearl River region is one exception to this. There we find that CLM0 minimum temperatures are about 1 K higher than the BATS counterpart in the winter, indicating a shift upwards to warmer temperatures over the full diurnal cycle. This could partially explain the similarity between the CLM0 simulations and observed temperature values in this region. Further possible explanations for the warmer temperatures in CLM0 are discussed in the following section.

4.3 Surface energy budget

An investigation of the energy partitioning at the surface can lend some insight into the differences between the surface temperature and precipitation simulations in the two schemes. Figure 4 illustrates the differences in the incoming surface solar radiation and cloud liquid water path between the CLM0 and BATS runs. We use cloud liquid water path as opposed to cloud cover fraction in order to assess the overall impact of clouds on the surface radiation budget and avoid the use of the cloud fraction overlap scheme used in the RegCM (Briegleb, 1992). The minimum, maximum, and average monthly incoming solar radiation observed during the period of 1984–1990 is included for comparison based on global 2.5° resolution data derived from the International

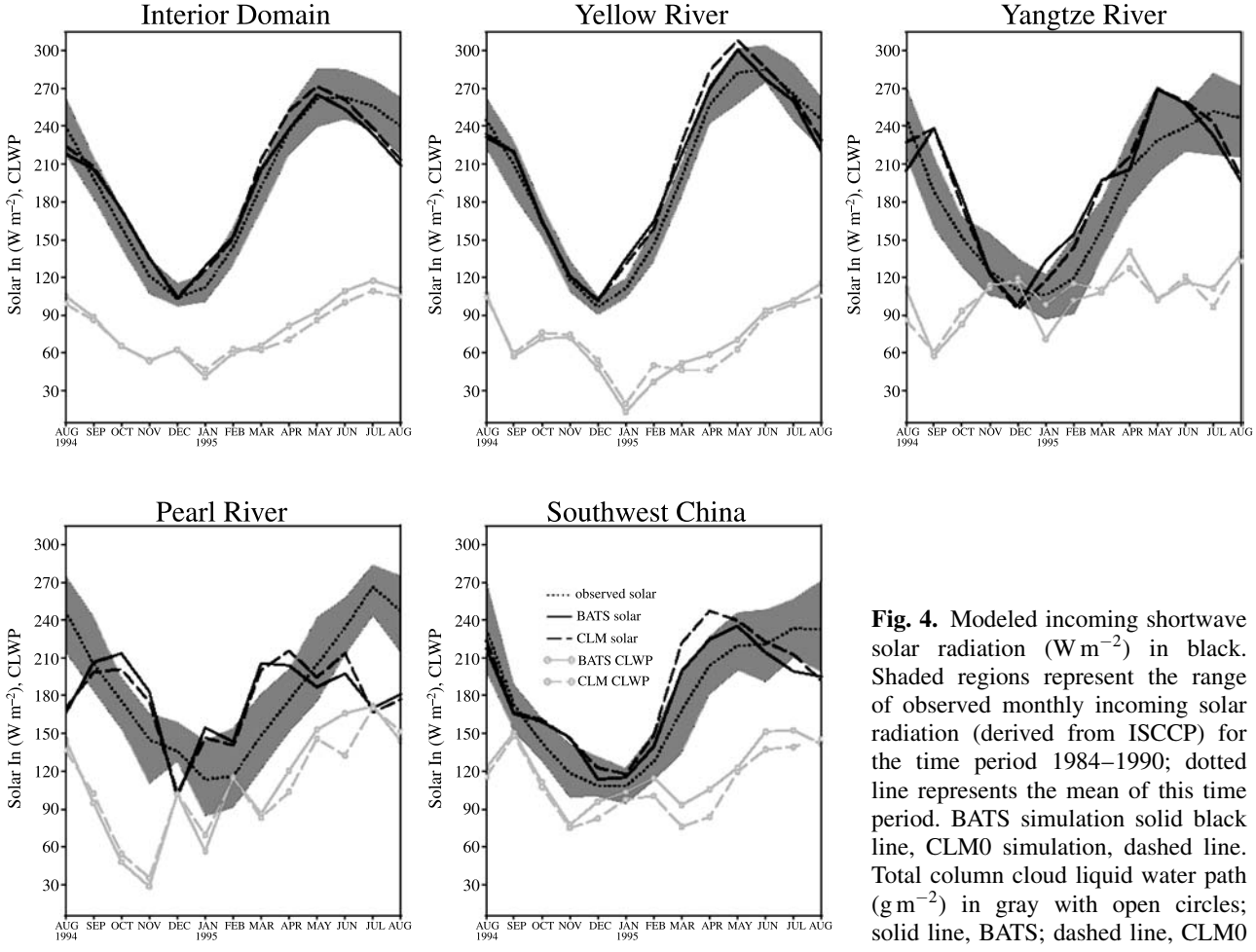

Fig. 4. Modeled incoming shortwave solar radiation (W m^{-2}) in black. Shaded regions represent the range of observed monthly incoming solar radiation (derived from ISCCP) for the time period 1984–1990; dotted line represents the mean of this time period. BATS simulation solid black line, CLM0 simulation, dashed line. Total column cloud liquid water path (g m^{-2}) in gray with open circles; solid line, BATS; dashed line, CLM0

Satellite Cloud Climatology Project (ISCCP) (Bishop and Rossow, 1991) and interpolated to the model grid. Typically, the annual surface solar radiation cycle reaches a minimum in December or January and a maximum in May. The onset of the East Asia monsoon causes this relatively early surface solar radiation maximum because the large cloud liquid water amounts during the summer reduce the amount of solar radiation that reaches the surface.

The modeled seasonal cycle matches the observed values fairly well over the interior domain and over most regions. The Pearl River region was a problematic region in the Giorgi et al. (1999) simulation, as the modeled radiation was over predicted by the model by approximately $90\,\mathrm{W\,m^{-2}}$ from the mean observed radiation in spring 1995. In our simulation, the incident radiation is still over predicted during this time period but the bias is reduced to approximately $60\,\mathrm{W\,m^{-2}}$ due to an increase in cloud cover attributed to the cloud and precipitation scheme of Pal et al. (2000). On the whole, the CLM0 and BATS values of incoming solar radiation are quite similar and differences between the two simulations can be explained by differences in cloud liquid water. For example, over the interior domain, the CLM0 simulates slightly higher incident radiation than the BATS simulation during the spring and summer. These increases in solar radiation are concomitant with decreases in cloud liquid water amount. Similar relationships are noted in other regions as well.

Figure 5 depicts the seasonal cycle of the surface energy budget for three components: the absorbed solar radiation, and the sensible and

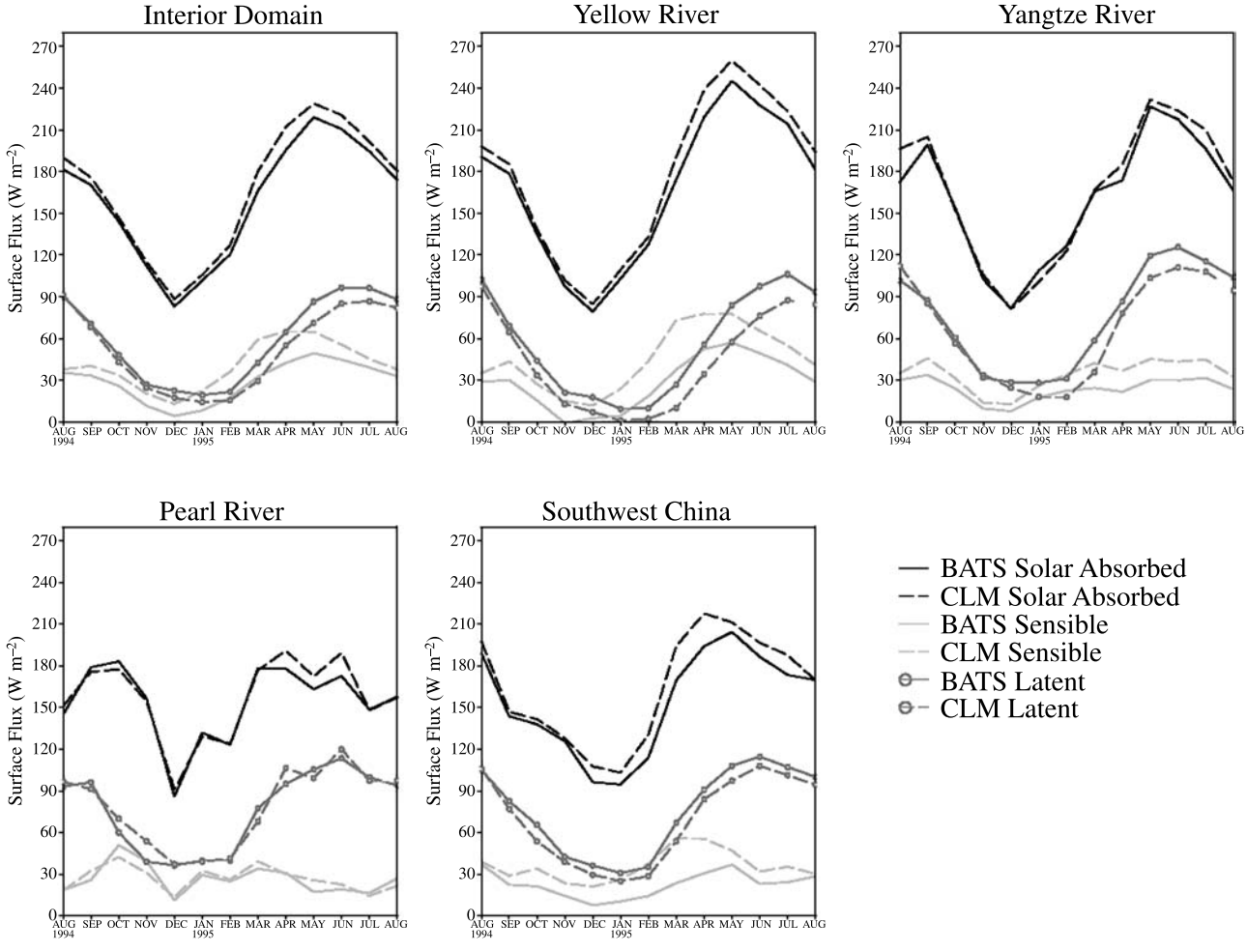

Fig. 5. Simulated surface energy balance (units, $\mathrm{W\,m^{-2}}$). For all fluxes, BATS represented by solid line and CLM0 by dashed line. Absorbed shortwave solar radiation in black, sensible heat in grey, and latent heat in black with open circles

latent heat fluxes. (Note that positive values for sensible and latent heat indicate a loss of energy from the land surface to the atmosphere.) We examine the absorbed solar radiation because it depends on surface albedo and therefore could cause surface temperature differences between BATS and CLM0. Alternatively, these other components of the surface energy balance could explain the origin of the surface temperature differences between the two simulations. Averaged over the annual cycle, CLM0 absorbs approximately $7\,W\,m^{-2}$ more than BATS. While some of this effect is due to additional incoming solar radiation in the CLM0 runs, the increase in the incoming solar ($4\,W\,m^{-2}$) is less than the absorbed solar difference ($7\,W\,m^{-2}$), indicating that the lower albedos in CLM0 are also likely responsible for the extra $3\,W\,m^{-2}$ of absorbed radiation.

During the summer months, CLM0 receives up to $5–10\,W\,m^{-2}$ more incoming radiation and absorbs $8–12\,W\,m^{-2}$ more than BATS due to lower CLM0 albedos in the visible range. However, this additional absorption of energy is not reflected in the surface temperatures. Generally, the CLM0 surface temperatures are close to if not lower than those of the BATS simulations during the summer.

As previously discussed, CLM0 predicts relatively higher surface temperatures than BATS during the winter months, although these periods are not matched by higher calculated values of incident solar radiation by CLM0. The amount of incoming solar radiation predicted by CLM0 is about $2–10\,W\,m^{-2}$ less than BATS, with the exception of Southwest China. However, even though CLM0 receives less incoming solar radiation at the surface, it still absorbs approximately $4\,Wm^{-2}$ more radiation over the interior domain and between $1–10\,W\,m^{-2}$ in other regions (except the Yangtze River region). This additional absorption of energy may contribute to an increase in winter surface temperatures, however the relationship between absorbed radiation and temperature is not consistent between the summer and winter seasons.

The increase in radiation absorbed in CLM0 is likely due to reduced albedos. There is a seasonal component to the albedo differences (not shown), with higher differences in albedo during the winter. The CLM0 albedo is approximately 0.12 less than BATS during the winter over the interior domain, which is probably due to the presence of less snow in the CLM0 runs, thereby reducing the shortwave direct component of the albedo. Most other regions see a similar seasonal cycle, and regions with greater amounts of snow cover in the BATS simulations show a greater albedo difference (e.g. the Yellow River region) and this could contribute to the winter temperature differences (see Section 4.4).

Another important factor in understanding changes in surface temperatures is the drag coefficient. In general, CLM0 has higher drag coefficients over land than BATS. The greater drag coefficients increase the amount of energy transferred away from the surface of the Earth by increasing the vertical mixing and surface energy fluxes. Variations in the surface roughness length, which depends on vegetation type and snow cover, can cause nonlinear changes in the drag coefficient. For example, drag coefficients over the northern regions (the Yellow and Yangtze River regions) tend to be slightly lower than in the southern regions (the Pearl River, Southwest China, and Southeast Asia regions). This is due to the presence of tropical vegetation and other forested ecosystems in the southern regions, which have higher surface roughness lengths. Additionally, the roughness length of snow varies between the two simulations; the BATS snow roughness length of 0.004 m is increased to 0.024 m in CLM0. Although CLM0 has less snow than its BATS counterpart (see Section 4.4), it has greater surface roughness during the winter particularly in the regions with larger amounts of snow (such as Southwest China).

BATS and CLM0 partition the absorbed radiation into sensible and latent heat fluxes quite differently (Table 3 and Fig. 5). The seasonal cycles of these variables include a minimum sensible heat flux in the early winter months (November or December) and a maximum in the late spring and early summer months (March to May). The latent heat flux peak tends to lag the sensible heat flux peak by a few months. This is due to the onset of the Asian monsoon season (see precipitation, Fig. 2). Once the summer rains begin, the latent heat relative to the sensible heat increases due to an increase in surface moisture.

With the exception of the Pearl River region, for all months that CLM0 produces sensible

Table 3. Differences in surface energy balance components. Values represent the difference between CLM0 and BATS simulations (CLM0-BATS); units are in $W\,m^{-2}$. Positive values indicate that CLM0 values are greater than BATS values, while negative values indicate that BATS has higher fluxes

	Interior Domain	Yellow River	Yangtze River	Pearl River	Southwest China
Annual					
Incoming Solar	3.79	3.59	0.64	0.96	8.11
Absorbed Solar	7.42	9.89	4.84	4.05	9.95
Sensible Heat	11.97	18.63	11.04	0.04	13.95
Latent Heat	−7.79	−14.09	−8.23	3.55	−7.06
DJF					
Incoming Solar	−1.92	−3.38	−9.86	−2.47	6.93
Absorbed Solar	4.35	5.77	−4.01	1.07	12.04
Sensible Heat	13.29	17.94	8.45	0.69	17.43
Latent Heat	−6.04	−8.91	−9.21	2.30	−6.36
JJA					
Incoming Solar	6.97	6.84	5.04	9.27	9.12
Absorbed Solar	8.90	11.82	8.69	10.77	10.72
Sensible Heat	8.03	26.05	11.89	1.18	8.44
Latent Heat	−10.17	−18.00	−10.73	3.77	−5.43

fluxes that are 10–20 $W\,m^{-2}$ higher than BATS, while latent heat fluxes from CLM0 are uniformly lower. These lowered latent heat fluxes may feed back to a reduction in simulation precipitation in for CLM0. Further discussion of the latent heat flux difference is presented below.

Table 4. Differences in surface water balance components. Values represent the difference between CLM0 and BATS simulations (CLM0-BATS); units in accumulated cm over the time of one month. Positive values indicate that CLM0 values are greater than BATS values, while negative values indicate that BATS has higher values. Surface storage indicates the amount of water entering the land surface (precipitation-total evapotranspiration-runoff)

	Interior Domain	Yellow River	Yangtze River	Pearl River	Southwest China
Annual					
Precipitation	−0.30	−0.05	0.06	−0.47	−1.21
Total Evapotranspiration	−0.82	−1.49	−0.86	0.37	−0.75
Canopy Evaporation	0	−0.03	0.01	−0.05	−0.05
Ground Evaporation	−1.31	−1.19	−1.31	−1.07	−1.65
Transpiration	0.53	−0.23	0.50	1.58	1.01
Runoff	0.84	0.96	1.45	0.88	0.53
Surface Storage	−0.32	0.48	−0.53	−1.72	−0.99
DJF					
Precipitation	0.15	0.43	1.24	0.24	−1.60
Total Evapotranspiration	−0.62	−0.93	−0.94	0.24	−0.66
Canopy Evaporation	0.21	0.12	0.30	0.22	0.30
Ground Evaporation	−0.98	−0.95	−1.38	−0.74	−1.35
Transpiration	0.17	−0.09	0.16	0.81	0.42
Runoff	0.34	0.14	1.04	0.89	−0.13
Surface Storage	0.40	1.22	1.14	−0.89	−0.81
JJA					
Precipitation	−0.40	−0.94	0.19	−0.90	−0.27
Total Evapotranspiration	−1.07	−1.90	−1.14	0.39	−0.58
Canopy Evaporation	−0.21	−0.24	−0.19	−0.31	−0.37
Ground Evaporation	−1.74	−1.64	−1.70	−1.53	−1.83
Transpiration	0.94	0.05	0.83	2.32	1.68
Runoff	1.50	1.67	2.38	0.84	1.55
Surface Storage	−0.83	−0.71	−1.05	−4.48	−1.25

4.4 Surface water budget

Differences in the surface water budget between the CLM0 and BATS simulations are presented in Table 4, including precipitation, total evapotranspiration and its three components, and surface runoff. Here we describe the different components of the water balance and their relationships. As detailed above, the BATS simulation produces slightly more precipitation (<10%) than the CLM0 simulations in both the annual mean and in the summer months.

Even though BATS receives more precipitation, CLM0 simulates more runoff than BATS. For most regions and months of the simulation, the runoff of CLM0 is ∼30% of the incident precipitation whereas BATS is typically 20–25%. This increase in runoff is also noted by Bonan et al. (2002) and Zeng et al. (2002) and is likely due to more efficient response of the CLM0 runoff parameterization to precipitation and snowmelt.

As also noted in the discussion of the energy budget, CLM0 simulates less latent heat flux (or evapotranspiration) than the BATS simulation. In Fig. 6, the evapotranspiration components (ground evaporation, canopy evaporation and transpiration) are broken out to provide further insight into the latent heat flux partitioning. Canopy evaporation, arising from the evaporation of intercepted water in the vegetation canopy, has a slight seasonal cycle that follows precipitation. In both models, the canopy intercepts and evaporates 12–17% of the incoming precipitation. This term is slightly larger for CLM0 in winter and for BATS in summer.

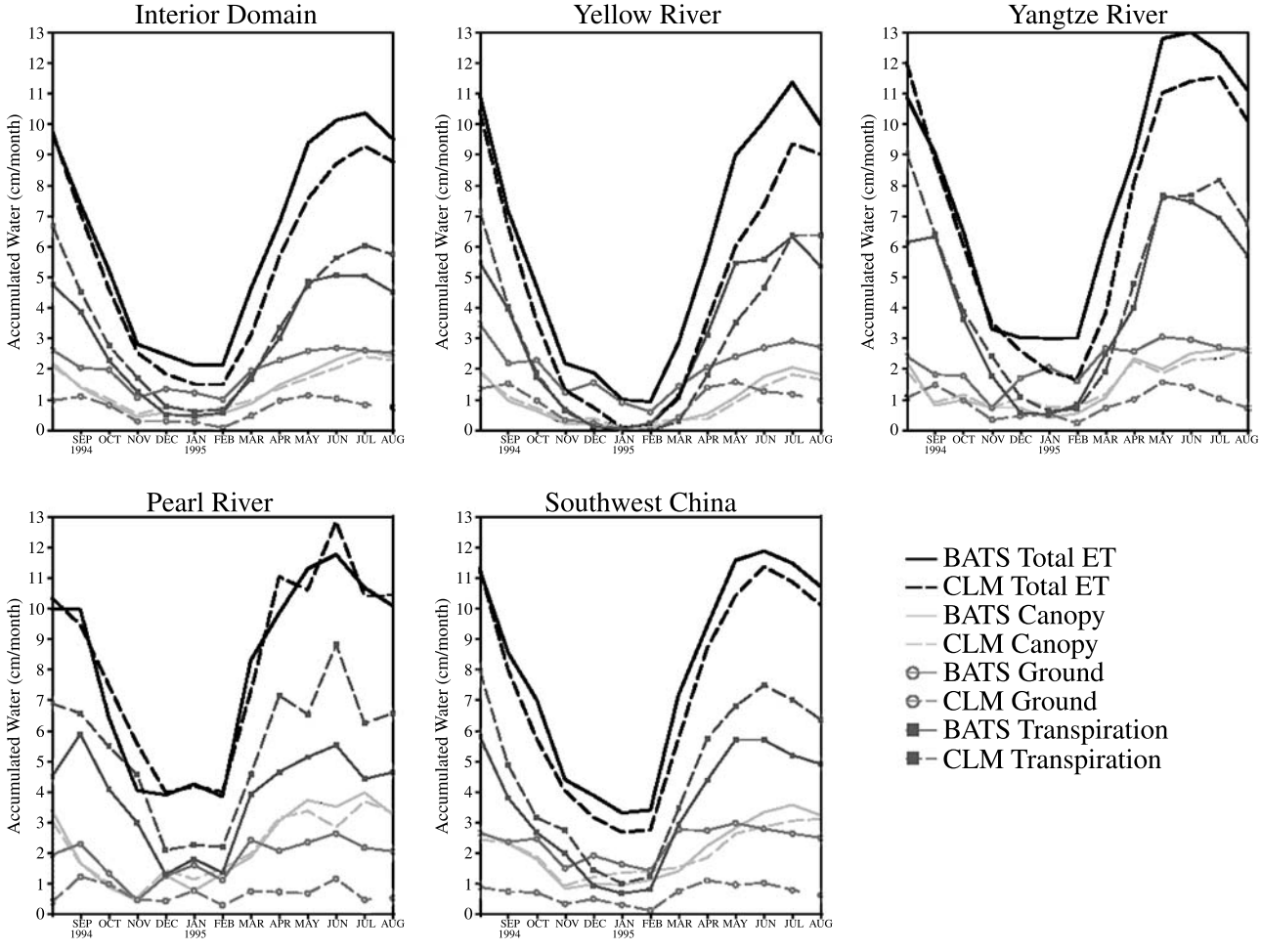

Fig. 6. Partitioning of evapotranspiration (units, accumulated cm of water). For all components, BATS represented by solid line and CLM0 by dashed line. Accumulated total evapotranspiration in black, canopy evaporation in grey, transpiration in black with solid squares, and ground evaporation in black with open circles

Ground evaporation is consistently less in CLM0 compared to BATS by about 60 to 70 percent. Ground evaporation in CLM0 is from a very thin surface layer that more readily dries out and therefore reduces evaporation compared to that from the upper soil layer in BATS. Similar reductions in ground evaporation were also noted by Bonan et al. (2002) and Zeng et al. (2002). Transpiration is a significant component of the latent heat flux during the growing season and has a similar seasonal cycle to that of temperature. It accounts for an annual average of about 46 percent of the amount of evaporated water in the BATS run and 62 percent in the CLM0 run.

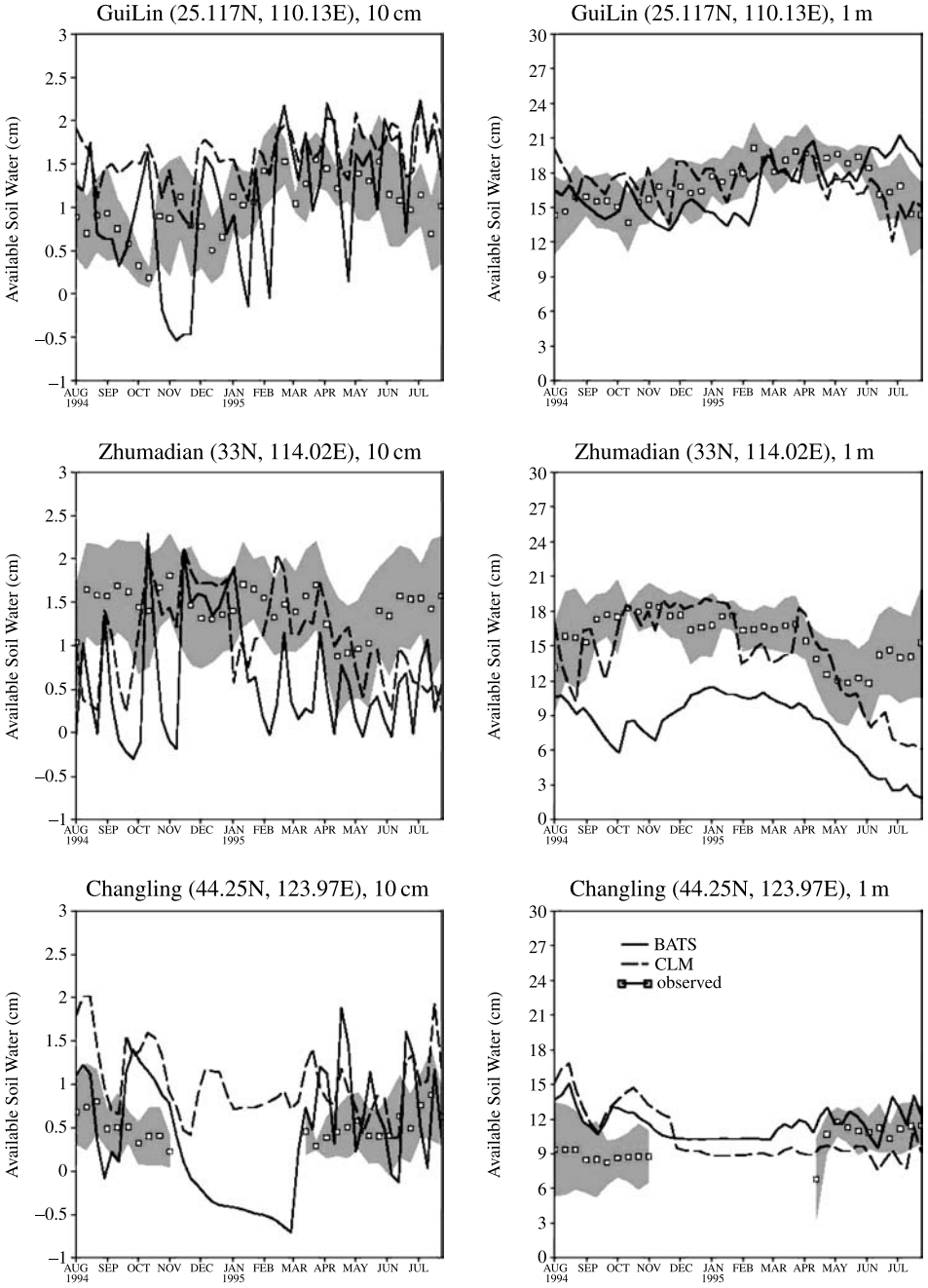

Fig. 7. Average observed (1981–1991; Robock et al., 2000), BATS and CLM plant available soil water (cm) for three observation sites in China: 1) Guilin, located in the Pearl River region, at 10 cm and 1 m depths, 2) Zhumadian, located in the Yangtze River region at 10 cm and 1 m depths, and 3) Changling, located north of the Yellow River region, at 10 cm and 1 m depths. For the observed 10 cm and 1 m data, ± one standard deviation is shown in the shaded areas

Particularly in the northern regions, the contribution of transpiration is at a maximum in the summer months and at a minimum in the winter months. In general, CLM0 partitions more of the total evaporation into transpiration than its BATS counterpart, likely due to the reduced ground evaporation and the revised stomatal conductance scheme.

The changes in partitioning of these fluxes also affect the soil water. We compared model output with several different stations within the model domain, based on the soil moisture data compiled by Robock et al. (2000) for the Global Soil Moisture Data Bank. Compared to other mid-latitude locations that normally experience a summertime drying when evapotranspiration exceeds precipitation, China has a relatively low-amplitude seasonal cycle of soil moisture because soil water is replenished during the Asian summer monsoon (Robock et al., 2000). Figure 7 compares the model results for plant available soil moisture (cm) at three individual stations and two depths: the top 10 cm and top 1 m of soil. Plant available soil moisture is the amount of soil water less the amount of soil water where wilting occurs (or the wilting point); therefore values below zero indicate vegetation cannot uptake water and transpiration ceases. To determine plant available soil moisture, observed wilting points are used for station data (Robock et al., 2000) and model wilting points (based on soil type and texture) are used for BATS and CLM0 simulations.

Observations were collected approximately every 10 days between 1981 and 1991 (Entin et al., 1999; Robock et al., 2000). Although these measurements do not match our study period, we show the 11-year seasonal average as representative of the soil moisture behavior in the region. Additionally, we show $\pm$ one standard deviation of the observed data to indicate the range of data collected during this time period. The measured soil depths correspond well with CLM layers, but the BATS root zone is often greater than the 1 m limit imposed by the data. Therefore, the BATS root zone soil moisture is normalized by the rooting depth in order to get a soil moisture value at the 1 m depth. It should be noted that at times, the model land use type in the models, which is often forested, does not correspond with the observational stations that are typically grassland and/or agriculture.

The first site, Guilin, is located within the Pearl River region. The modeled results vary monthly over a range that is consistent with or slightly larger than the standard deviation for the observations, shown as shaded regions in Fig. 7. At the 10 cm level, modeled surface soil moisture values during the winter and early spring at Guilin are within the range of observed data for both models. BATS surface moisture is much more variable than CLM, often predicting values that are well outside the range of standard deviation. At the 1 m depth, when fine temporal scale variability is less pronounced, both CLM0 and BATS reproduce the soil moisture amount well at this location. However, CLM is able to capture the late summertime soil drying occurring in this region after the summer monsoon has passed, which BATS is unable to do.

The second site, Zhumadian, is located in the Yangtze River region. At this site, CLM0 more closely reproduces the observed soil moisture than BATS at both the 10 cm and 1 m levels, although surface soil moisture is under predicted in the fall and summer. However, both models simulate a summer drying in the latter portion of the simulation that is not present in the observations. Unlike the Pearl River region, it appears that the observed soil moisture in this region is restored by precipitation from the Asian monsoon, as similar trends are noted in observations from other field sites located in this region (not shown). The models may not be capturing this restoration because of problems with the precipitation simulation, such as the excessive northward displacement of the monsoonal front that causes precipitation to occur earlier than the observations indicate (Section 4.1). This could lead to more drying in the simulated soil because of the lack of precipitation at the correct time in the model. Another possible explanation for the drier soils in the latter half of the simulation versus the wetter August at the beginning of the simulation may be the soil moisture initialization. While we did account for a two-month model spin-up, this may not be sufficient time for the soil moisture to equilibrate and may be causing the drier summer at the end relative to the beginning of the simulation.

The third site, Changling, is located slightly to the north of the Yellow River region. In the top 10 cm, BATS is predicting available soil water that is close to the observed values, while CLM0 predicts slightly higher values. At a 1 m depth, both models over predict the soil moisture in the beginning of the simulation. In March, when observations are available after the thawing of the ground, BATS more closely matches the observations by predicting a wetter soil at this site. It is possible that the drier CLM0 soil moisture at this northern site may be related to the snow simulations and the under estimation of snow, as discussed further below.

Overall, Fig. 7 shows that CLM0 has wetter surface soil (10 cm) than BATS at most of these sites analyzed as well as throughout the model domain. This is consistent with the new parameterization and reduction of ground evaporation in CLM0. At the observation sites considered, CLM0 is wetter than BATS in the deeper soil layer for two of the three locations. On the whole, though, the relative magnitude of BATS vs. CLM soil moisture column varies spatially and temporally. As shown in the storage term in Table 4, BATS is storing more water than CLM0 in the soil column in the summertime, while during the winter and throughout the annual cycle, the storage is more variable. Despite these variations, Fig. 7 (and other station locations not shown) indicates that CLM0 can reasonably simulate the seasonal cycle of soil moisture and mostly improves the deeper soil moisture simulation compared to BATS, particularly in the southern and central portions of the model domain.

Another important component of the hydrologic cycle and the land surface simulation is the presence and cycling of snow. In Fig. 8, we compare the total snow area of the inner domain as observed and simulated in both the BATS and CLM experiments. The observed snow area is derived from the National Snow and Ice Data Center Northern Hemisphere weekly climatological snow cover (Armstrong and Brodzik, 2002). This data set is based on the NOAA/NESDIS weekly snow cover charts derived from manual interpretations of AVHRR, GOES, and other visible band satellite data. We compare this data with the areal extent of snow in the BATS and CLM0 simulations and find that both models underestimate the amount of snow present in the inner

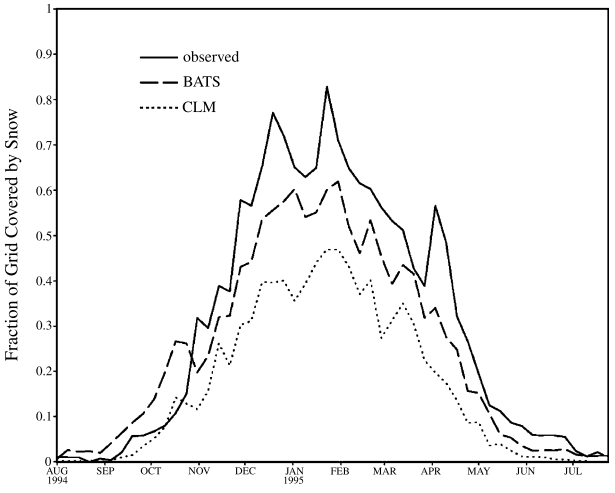

Fig. 8. Snow. Observed (Armstrong and Brodzik, 2002) and modeled (BATS and CLM) areal extent of snow cover over the inner model domain

domain. This underestimate is especially evident in the CLM0 simulation. However, it should be noted that both models do not account for the sub-grid orographic representation of topography in the snowfall, therefore an under prediction of snow might be expected in complex terrain (Giorgi et al., 2003).

Because the complete suite of snow variables was not output in the land surface simulations, we use the lowest model level air temperatures and RegCM snowfall criteria (2.2 degrees K above the freezing temperature) to compare the amount of snowfall occurring in BATS and CLM0. Based on these precipitation comparisons, BATS produces more snowfall than CLM0 and this probably contributes to the greater areal extent of snow in BATS compared to CLM0. However, further study will be required to compare the loss rates (i.e. snowmelt and snow sublimation) and evaluate if these factors are also contributing to the reduction of snow in CLM0.

The snow and temperature results indicate a feedback between snow cover and air temperatures. We speculate that because BATS has more snow, the surface albedo increases, the amount of absorbed radiation decreases, and surface temperatures decrease. In turn, cooler surface and atmospheric temperatures will produce more snowfall vs. rainfall, which can further increase the amount of snow on the ground in BATS. We believe that this mechanism may provide a strong contribution to the surface temperature and snow

differences between CLM0 and BATS noted in Figs. 3 and 8. However, Fig. 8 clearly indicates that the simulation of snow by CLM0 coupled to the RegCM is deficient over this domain, and this aspect of the model will need to be improved for future applications of the RegCM/CLM0.

5. Discussion and conclusions

We find that the newly coupled RegCM/CLM0 can reproduce the general features of seasonal cycle of temperature, precipitation and other land surface parameters. We compare the effects of two different land surface parameterizations within a regional climate model (RegCM) for a year-long simulation over East Asia. In general, the change of land surface scheme does not have a strong impact on precipitation, which is similar between the two schemes. With respect to temperature, the CLM0 leads to substantially higher surface temperatures in the winter, which decreases the RegCM cold winter bias over the region. This reduction in the cold bias is at least partially due to the presence of less snow in the CLM0 and the associated snow-temperature feedbacks. The main effect of the land surface scheme is on the simulation of the surface hydrologic cycle, a result noted and validated in other CLM studies (Bonan et al., 2002; Zeng et al., 2002; Dai et al., 2003). A possible mechanism that explains our results for the warm season is the following. Overall, less water enters the soil in the CLM0 simulation than in the BATS simulation as a result of a slight decrease in precipitation and greater runoff efficiencies in CLM0. Despite a lower precipitation input, the soil water contents in CLM0 are higher than in BATS because of much reduced ground evaporation rates. Therefore, BATS and CLM0 show very different partitioning of water across the different components of the surface water budget and substantially different Bowen ratios. A limited comparison with observations indicates that the soil water contents simulated by CLM0 are more realistic than the BATS counterpart.

During the winter months, a major difference between the CLM0 and BATS experiments is the simulation of snow amounts. In fact, BATS produces a larger snow accumulation on the surface than CLM0, which is also in greater agreement with observations. The reduced CLM0 snow cover causes a reduction in surface albedo and increases the amount of radiation absorbed. This, in turn, increases the surface radiative energy fluxes, leading to higher winter temperatures in CLM0. The snow simulation appears to be the weakest aspect of the RegCM-CLM0 coupling and further investigation of the mechanisms of snow formation and loss may help to improve this aspect of the model for future application. Overall, however, except for the snow simulation the coupling with CLM0 leads to an improvement of several aspects of the surface energy and water cycles. However, longer-term simulations in different regional settings should be performed to evaluate the robustness of these results.

Acknowledgements

This work was completed under NASA Earth System Science Fellowship NGT5-50330 to A. Steiner. The assistance of Yongjui Dai and Muhummed Shaikh of Georgia Tech and Xunqiang Bi of the ICTP is greatly appreciated. We would also like to thank Mingquan Mu for his assistance in using the Chinese soil moisture data from the Global Soil Moisture Data Bank (http://climate.envsci.rutgers.edu/soil_moisture/).

References

Adams JC, Lettenmaier DP (2003) Adjustment of global gridded precipitation for systematic bias. J Geophys Res 108: 4257, doi: 10.1029/2002JD002499

Anthes RA (1977) A cumulus parameterization scheme utilizing a one-dimensional cloud model. Mon Wea Rev 105: 270–286

Anthes RA, Hsie EY, Kuo YH (1987) Description of the Penn State/NCAR Mesoscale Model Version 4 (MM4), NCAR Technical Note, NCAR/TN-282+STR, National Center for Atmospheric Research, Boulder, Colorado

Armstrong RL, Brodzik MJ (2002) Northern Hemisphere EASE-Grid weekly snow cover and sea ice extent, Version 2. Boulder, CO, USA: National Snow and Ice Data Center, CD-ROM

Bishop JKB, Rossow WB (1991) Spatial and temporal variability of global surface solar irradiance. J Geophys Res 96: 16839–16858

Bonan GB (1996) A land surface model (LSM version 1.0) for ecological, hydrological, and atmospheric studies. NCAR Technical Note, NCAR/RN-417+STR

Bonan GB, Oleson KW, Vertenstein M, Levis S, Zeng X, Dai Y-J, Dickinson RE, Yang Z-L (2002) The land surface climatology of the community land model coupled to the NCAR Community Climate Model. J Climate 15: 3123–3149

Briegleb BP (1992) Delta-Eddington approximation for solar radiation in the NCAR Community Climate Model. J Geophys Res 97: 7603–7612

Brutsaert W (1982) Evaporation in the atmosphere. Dordrecht: Kluwer Academic Publishers, 299 pp

Clapp RB, Hornberger GM (1978) Empirical equations for some soil hydraulic properties. Water Resour Res 20: 682–690

Collatz GJ, Ball JT, Grivet C, Berry JA (1991) Physiological and environmental regulation of stomatal conductance, photosynthesis and transpiration: a model that includes a laminar boundary layer. Agric Forest Meteorol 54: 107–136

Dai Y, Zeng QC (1996) A land surface model (IAP94) for climate studies. Part I: Formulation and validation in off-line experiments. Adv Atmos Sci 14: 433–460

Dai YJ, Zeng X, Dickinson RE, Baker I, Bonan GB, Bosilovich MG, Denning AS, Dirmeyer PA, Houser PR, Niu G, Oleson KW, Schlosser CA, Yang Z-L (2003) The common land model. Bull Amer Meteor Soc 84: doi: 10/1175/BAMS-84-8-1013

Deardorff J (1978) Efficient prediction of ground temperature and moisture with inclusion of a layer of vegetation. J Geophys Res 83: 1889–1903

Dickinson RE (1988) The force-restore model for surface temperatures and its generalizations. J Climate 1: 1086–1097

Dickinson RE, Henderson-Sellers A, Kennedy PJ (1993) Biosphere-Atmosphere Transfer Scheme (BATS) version 1e as coupled to the NCAR Community Climate Model. NCAR Technical Note NCAR/TN-387+STR, 72 p

Entin JK, Robock A, Vinnikov KY, Zabelin V, Liu S, Namkhai A, Adyasuren T (1999) Evaluation of the Global Soil Wetness Projection soil moisture simulations. J Meteor Soc Jpn 77: 183–198

Farquhar GD, von Caemmerer S, Berry JA (1980) A biochemical model of photosynthetic CO_2 assimilation in leaves of C_3 species. Planta 149: 78–90

Giorgi F, Bates GT (1989) On the climatological skill of a regional model over complex terrain. Mon Wea Rev 117: 2325–2347

Giorgi F, Marinucci MR, Bates GT (1993a) Development of a second generation regional climate model (RegCM2). Part I: Boundary-layer and radiative transfer processes. Mon Wea Rev 121: 2794–2813

Giorgi F, Marinucci MR, Bates GT, De Canio G (1993b) Development of a second generation regional climate model (RegCM2). Part II: Convective processes and assimilation of lateral boundary conditions. Mon Wea Rev 121: 2814–2832

Giorgi F, Shields C (1999) Tests of precipitation parameterizations available in the latest version of the NCAR regional climate model (RegCM) over continental U.S. J Geophys Res 104: 6353–6375

Giorgi F, Huang Y, Nishizawa K, Fu C (1999) A seasonal cycle simulation over eastern Asia and its sensitivity to radiative transfer and surface processes. J Geophys Res 104: 6403–6423

Giorgi F, Bi X (2000) A study of internal variability of a regional climate model. J Geophys Res 105: 29503–29521

Giorgi F (2002) Variability and trends of sub-continental scale surface climate in the twentieth century. Part I: observations. Clim Dynam 18: 675–691

Giorgi F, Francisco R, Pal J (2003) Effects of subgrid-scale topography and land use scheme on the simulation of surface climate and hydrology, Part I: Effects of temperature and water vapor disaggregation. J Hydrometeorol 4: 317–333

Grell G (1993) Prognostic evaluation of assumptions used by cumulus parameterizations. Mon Wea Rev 121: 764–787

Henderson-Sellers A, Dickinson RE (1993) Atmospheric-land surface fluxes. In: Jakeman AJ, Beck MB, McAleer MJ (eds) Modelling change in environmental systems. John Wiley and Sons, pp 387–405

Holtslag AAM, de Bruijin EIF, Pan HL (1990) A high resolution air mass transformation model for short-range weather forecasting. Mon Wea Rev 118: 1561–1575

Jarvis PG (1976) The interpretation of the variations in leaf water potential and stomatal conductance found in canopies in the field. Philos T Roy Soc B 273: 593–610

Kiehl JT, Hack JJ, Bonan GB, Boville BA, Briegleb BP, Williamson DL, Rasch PJ (1996) Description of the NCAR Community Climate Model (CCM3), NCAR Technical Note NCAR/TN-420+STR, 152 p., National Center for Atmospheric Research, Boulder, Colorado

Koster RD, Suarez MJ (1992) Modeling the land surface boundary in climate models as a composite of independent vegetation stands. J Geophys Res 97: 2697–2715

Lau KM, Li MT (1984) The monsoon of east Asia and its global associations – a survey. Bull Amer Meteor Soc 65: 114–125

Legates DR, Willmott CJ (1990) Mean seasonal and spatial variability in gauge-corrected, global precipitation. Int J Climatol 10: 111–127

Manabe S (1969) Climate and ocean circulation. I. The atmospheric circulation and the hydrology of the earth's surface. Mon Wea Rev 97: 739–774

New MG, Hulme M, Jones PD (1999) Representing twentieth-century space time climate variability, I., Development of a 1961–1990 mean monthly terrestrial climatology. J Climate 12: 829–856

New MG, Hulme M, Jones PD (2000) Representing twentieth-century space time climate variability, I., Development of a 1901–1996 mean monthly terrestrial climatology. J Climate 13: 2217–2238

Pal JS, Small EE, Eltahir EAB (2000) Simulation of regional-scale water and energy budgets: Representation of subgrid cloud and precipitation processes within RegCM. J Geophys Res 105: 29579–29594

Philip JR (1957) Evaporation, and moisture and heat field in the soil. J Meteorol 14: 354–366

Robock A, Vinnikov KY, Srinivasan G, Entin JK, Hollinger SE, Speranskaya NA, Liu S, Namkhai A (2000) The global soil moisture data bank. Bull Amer Meteor Soc 81: 1281–1299

Sellers P (1985) Canopy reflectance, photosynthesis and transpiration. Int J Remote Sens 6: 1335–1372

Sellers PJ, Dickinson RE, Randall DA, Betts AK, Hall FG, Berry JA, Collatz GJ, Denning AS, Mooney HA, Nobre CA, Sato N, Field CB, Henderson-Sellers A (1997) Modeling the exchanges of energy, water and carbon between continents and the atmosphere. Science 275: 502–509

Stieglitz M, Rind D, Famiglietti J, Rosenzweig C (1997) An efficient approach to modeling the topographic control of surface hydrology for regional and global climate modeling. J Climate 10: 118–137

Trenberth KE, Olson JG (1992) ECMWF global analyses 1979–1986: Circulation statistics and data evaluation, NCAR Technical Report, TN-300+STR, 94 pp., National Center for Atmospheric Research, Boulder, Colorado

Yang Z-L, Dickinson RE (1997) Description of the Biosphere-Atmosphere Transfer Scheme (BATS) for the Soil Moisture Workshop and evaluation of its performance. Global Planet Change 13: 117–134

Zeng X, Dickinson RE (1998) Effect of surface sublayer on surface skin temperature and fluxes. J Climate 11: 537–550

Zeng X, Zhao M, Dickinson RE (1998) Intercomparison of bulk aerodynamic algorithms for the computation of sea surface fluxes using the TOGA COARE and TAO data. J Climate 11: 2628–2644

Zeng X, Shaikh M, Dai YJ, Dickinson RE, Myneni R (2002) Coupling of the Common Land Model to the NCAR Community Climate Model. J Climate 15: 1832–1854

Zilitinkevich SS (1970) Dynamics of the atmospheric boundary layer. Leningrad Gidrometeor, 291 pp

Authors' addresses: Allison L. Steiner* (e-mail: asteiner@mature.berkeley.edu), Robert E. Dickinson, William L. Chameides, School of Earth and Atmospheric Sciences, Georgia Institute of Technology, Atlanta, GA 30332-0340, USA; Jeremy S. Pal, Filippo Giorgi, Physics of Weather and Climate Group, International Centre for Theoretical Physics, Trieste 34014, Italy; *Present address: Department of Environmental Science, Policy and Management, University of California, Berkeley, 151 Hilgard Hall #3110, CA 94720-3110, USA.